CRYSTAL GROWTH & DESIGN

Article

pubs.acs.org/crystal

Persistent Reverse Enantiomeric Excess in Solution during Viedma Ripening

Laura Spix, Anthonius H. J. Engwerda, Hugo Meekes,* Willem J. P. van Enckevort, and Elias Vlieg

Radboud University, Institute for Molecules and Materials, Heyendaalseweg 135, 6525 AJ Nijmegen, The Netherlands

ABSTRACT: During Viedma ripening experiments on alanine 4-chlorobenzenesulfonic acid, the solution shows a small enantiomeric excess ee_l with the reverse sign as compared to the solid state enantiomeric excess. This reverse solution ee_l is persistent, even after the deracemization is complete, as long as the grinding is maintained. A model that includes thermodynamic chiral clusters and their incorporation into larger crystals of the same chirality explains this behavior. The size of the reverse ee_l is in good agreement with the estimated subcritical cluster distribution calculated on the basis of a Boltzmann distribution and classical nucleation theory.

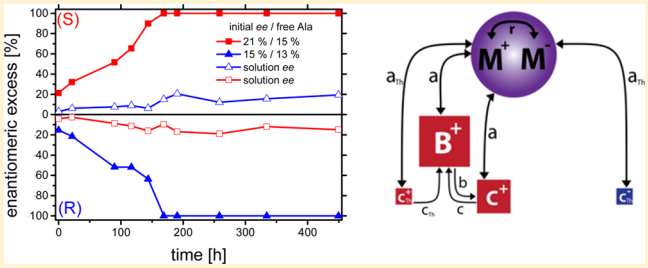

INTRODUCTION

Viedma ripening is a recent innovation in chiral purification methods.[1] In the process of Viedma ripening, chiral crystals are ground in contact with their saturated solution. Starting from a racemic conglomerate of left- and right-handed crystals, any small enantiomerical imbalance leads to an enantiomerically pure end state in the solids. Viedma ripening is thus a deracemization process instead of a resolution process, as 100% of the solids are converted into a single enantiomer. The outcome of the enantiomeric end state can be directed, for example, by adding a small amount of enantiomerically pure crystals at the start of the process. In the case of intrinsically chiral molecules, a racemization reaction in the solution is needed to convert the right-handed into the left-handed molecule and *vice versa*.

After the first discovery of this deracemization process for the achiral compound $NaClO_3$ by Viedma, several examples have been reported in the literature of achiral compounds that form chiral crystals and that undergo Viedma ripening.[1−6] Meanwhile, many examples of complete deracemization of intrinsically chiral molecules for which racemization in the solution is necessary have been reported as well.[7−21] It is quite well understood which requirements must be fulfilled to make Viedma ripening feasible and also how circumstances like solubility and grinding intensity influence the deracemization rate.[22] The details of the exact mechanism behind Viedma ripening, however, are still under debate.

Several models have been proposed. After the first deracemization experiments were conducted and published by Viedma[1] in 2005, Uwaha proposed a reaction type model to explain the process.[23] The model features chiral clusters of the intrinsically achiral compound being essential for the full and rapid deracemization. Later, when Viedma ripening was extended to the cases of intrinsically chiral compounds,[7] several alternative models to explain Viedma ripening for chiral molecules were reported.[24−29]

All of these proposed models yield the sigmoidal curves for the enantiomeric excess in time that are typically observed during Viedma ripening, which was taken as evidence for their correctness. The application of additives, however, recently was shown to change the sigmoidal curves to linear ones.[21] The best way to establish the true mechanism of Viedma ripening would be direct experimental evidence, for example, for the action of chiral clusters. Such experiments, however, are not easily conducted because the smallest particles in a slurry of crystals of different shapes and sizes need to be observed, which is difficult, if not impossible. Information thus has to come from more macroscopic observations.

Here, we report experiments on the enantiomeric excess (*ee*) in solution during deracemization. Earlier, Noorduin et al.[27] observed that, *during* grinding of an enantioenriched racemic conglomerate, but in the absence of racemization in the slurry, the solution obtains an *ee* with an opposite sign compared to the solids. Their model required the enantioselective incorporation of chiral clusters. A consequence of their explanation for this result was that, once the solid *ee* reaches 100%, this solution *ee* value becomes 0%. We find, however, that, even when deracemization is complete, the solution still has a reverse *ee*. We propose as an explanation for this observation the presence of very small, thermodynamically stable chiral clusters.

EXPERIMENTAL RESULTS

During Viedma ripening experiments on alanine 4-chlorobenzenesulfonic acid, we conducted stability experiments of the enantiomerically pure end state.[19] These experiments were started with enantiomerically pure alanine and 4-chloro-

Received: May 27, 2016
Revised: July 12, 2016
Published: July 12, 2016

DOI: 10.1021/acs.cgd.6b00804
Cryst. Growth Des. 2016, 16, 4752−4758

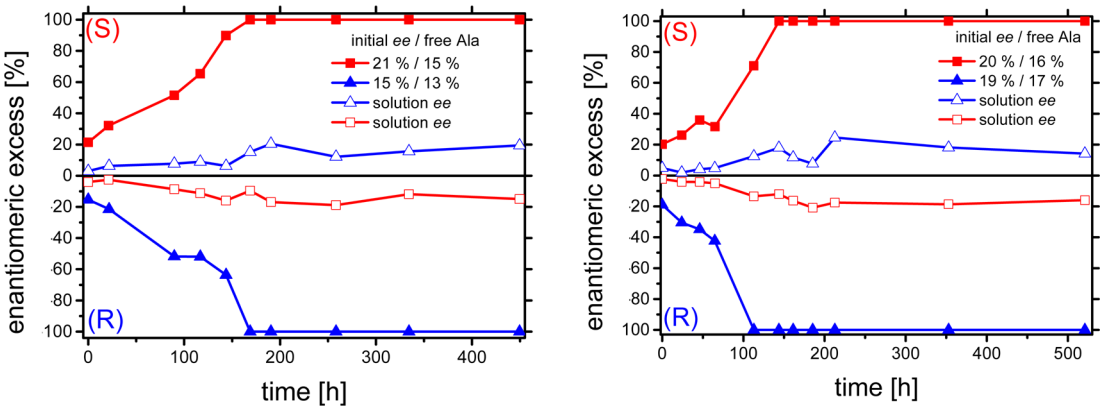

Figure 1. Attrition-enhanced evolution of solid-phase *ee* (filled symbols) and solution *ee* (open symbols) for alanine 4-chlorobenzenesulfonic acid. In all four cases, the solids samples and solution samples had opposite signs for their *ee*. The four separate experiments were conducted at 70 °C. Lines are a guide to the eye. The amount of free Ala is indicated as the weight percentage of excess alanine. The error in the *ee* values is estimated to be mainly determined by the sampling accuracy.

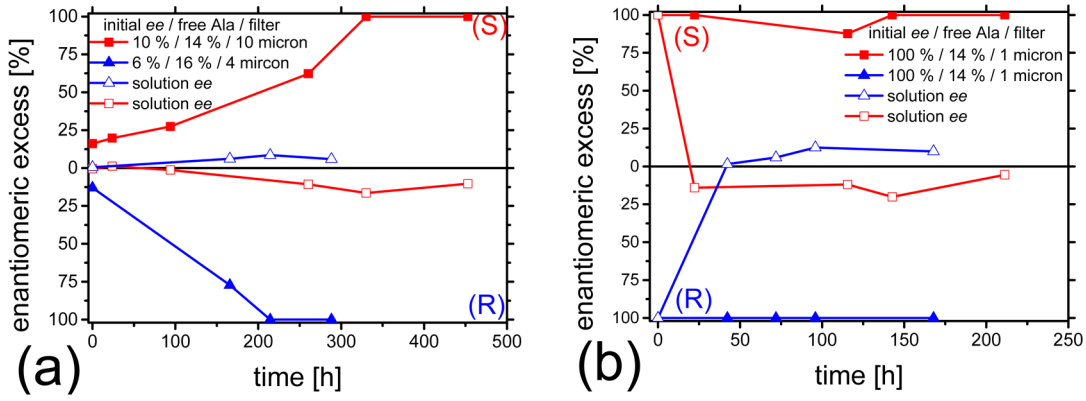

Figure 2. Attrition-enhanced evolution of solid-phase ee_s (filled symbols) and solution ee_l (open symbols) for alanine 4-chlorobenzenesulfonic acid. Experiments were conducted at 70 °C. Solution samples were taken in situ using cannula filters (pore size as indicated). Lines are a guide to the eye. The anomalous solid phase of *ee* = 90% at 115 h in (b) was caused by crystals that were stuck to the flask walls and were not ground. When the grinding was re-established, the system returned to the stable enantiomerically pure end state.

benzenesulfonic acid in a 10:9 ratio (see the section Experimental Details). The amount of all used chemicals was identical to a normal deracemization experiment, including the racemization catalyst, as described in the section on experimental details. We then found that the enantiomerically pure end state remains stable for at least 200 h.

In successive similar experiments, in addition to the solid state *ee*, we also checked the *ee* in the solution as a function of time. Because of racemization in the solution, the latter is expected to be 0%, but we surprisingly found the solution showed a distinct *ee* (between 15% and 20%) of the opposite sign compared to the solids. For these experiments, the samples were filtered over a P4 glass filter and the solution, including the washing solvent, was collected in a Büchner flask. Because of the fast drop in temperature of the solution, once removed from the experiment, the racemization stops and the solution *ee* is arrested. After evaporating the liquids completely, the resulting crystals from the solution phase and the solid phase were analyzed using chiral HPLC (see the Experimental Details for further information).

Figure 1 shows the enantiomeric excess of both the solution and the solid phase for four such deracemization experiments. The solution *ee* increased (ee_l = 2−5%) along with the solid-phase *ee* until the latter was enantiomerically pure. After that, the solution *ee* remained almost constant at around 15%. If some very small crystals or clusters would pass the filter during sampling, one would observe a nonzero *ee* in the solution of the same handedness as in the solid state. Thus, the observed opposite handedness of the solution cannot be explained by accidental sampling of solid material.

Gathering the solution *ee* sample by filtration bears the risk that, in the process, the crystals in the glass filter, when still in contact with the solution, can grow. Thereby, the solution would be deprived of the major enantiomer of the solid phase, resulting in an enantiomeric excess of the opposite handedness. This could explain the observed phenomenon. To rule out this effect, we went for an *in situ* method to obtain a crystal-free solution from a Viedma ripening experiment. For this, a 1 mL syringe was equipped with a poroplast cannula filter (10, 4, or 1 μm) and the solution was extracted, free of crystals, at 70 °C directly from the round-bottom flask (see the Experimental Details). With this sampling method, we again conducted complete Viedma ripening experiments (Figure 2a). We also started with enantiomerically pure crystals that were ground in a saturated racemizing solution (Figure 2b). For the first data point, both the solids and the solution have 100% *ee* because that sample was taken shortly before the racemization catalyst was added. The results of these experiments are in essence the same as the ones in Figure 1, thus confirming the persistent reverse solution *ee*.

DOI: 10.1021/acs.cgd.6b00804
Cryst. Growth Des. 2016, 16, 4752−4758

The racemization time to reach 50% *ee* for racemic alanine 4-chlorobenzenesulfonic acid at 70 °C at the concentrations given in the section Experimental Details is typically 1−1.5 h (see the Supporting Information to ref 19), which is fast as compared to the time scales in the steady state situation of Figure 2. Therefore, after having reached 100% *ee* in the solids, already in a relatively short time, the only monomers entering the solution as a result of the grinding are of the enantiomer of the solids and can, therefore, not explain the reverse solution *ee*.

MODEL CALCULATION

Failure of Simple Cluster Model. As mentioned before, Noorduin et al. already observed a reverse solution *ee* during grinding of an enantioenriched racemic conglomerate.[27] In their paper, a model was presented that agreed with the observation, and which was based on earlier work of Uwaha.[23] The model also predicted a reverse solution *ee* in the case of racemization in the solution. However, it predicts a 0% ee_l once the deracemization of the solids has completed. Here, we present an extension of this model to explain the presently observed persistent solution *ee* after complete deracemization. The extension involves thermodynamic clusters which are always present, even in a (nearly) equilibrium situation. The model used by Noorduin et al. contains four essential processes: (1) Ostwald ripening, (2) racemization in solution, (3) attrition of large crystals, and (4) enantioselective incorporation of chiral clusters. The model simplifies the crystal size distribution in the Viedma ripening process to merely two sizes: big crystals, containing B^+ and B^- molecules altogether for the two enantiomers, respectively, and small crystals or clusters formed by the attrition, containing C^+ and C^- molecules. Note that, in the original paper, the symbols *R* and *S* were used instead of + and −. The deracemization process was modeled by a set of rate equations with rate constants *a* for the growth and dissolution of crystals *B* and clusters *C* with monomers, *b* for the attrition of big crystals, *c* for the enantioselective incorporation of chiral clusters into big crystals, and *r* for the racemization in the solution. Uwaha already claimed that the enantioselective incorporation of chiral clusters into larger crystals was essential for the autocatalytic behavior of Viedma ripening, resulting in sigmoidal deracemization vs time plots.

The Noorduin model shows that, as soon as the Viedma ripening results in an increase of the solid-phase enantiomeric excess ee_s, the solution enantiomeric excess ee_l increases as well, but with opposite sign. As can be seen in Figure 3, the reverse ee_l increases with increasing ee_s until total deracemization is reached, after which ee_l rapidly decreases to zero and remains zero.

Figure 4 shows the ongoing processes according to this model once deracemization is complete. In the absence of solid material of the "−" type, a steady state situation is reached and the amounts of M^+ and M^- molecules have to be equal. This implies that the solution *ee* is predicted to be zero in this end situation. This model fails to explain the persistent reverse solution *ee* we have observed and report here.

Extended Model. The failure of the earlier model to explain the reversed solution *ee* after complete deracemization means that the model needs a modification. None of the earlier models has the right ingredient to explain our observation either. Here, we propose to extend the Noorduin model by including thermodynamic clusters, i.e., the very small clusters that are present in a (saturated) solution and that are formed

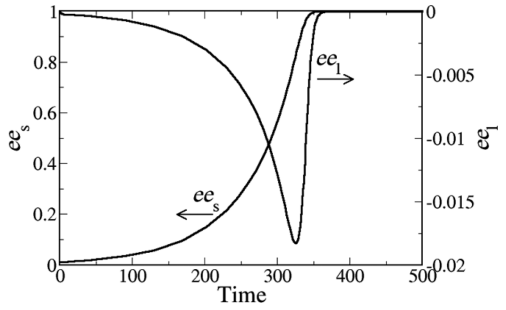

Figure 3. Enantiomeric excess ee_s and ee_l as a function of time in arbitrary units. Recalculated from Noorduin et al. (Supporting Information).[27]

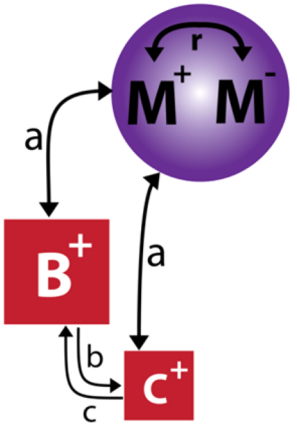

Figure 4. Final situation of a Viedma ripening experiment with just one enantiomer left in the solid phase according to the model of Noorduin et al.[27] B represents big crystals, C clusters, and M the solute in the solution phase. To label the two enantiomers, + and − signs are used. The process rate constants *a*, *b*, *c*, and *r* are explained in the main text.

and disappear by the spontaneous addition and removal of molecules. The model has already two crystal sizes, *B* and *C*, but these represent the effect of growth and attrition. Similar to the simplification of the crystal size distribution to two sizes, *B* and *C*, we will represent the total amount of molecules in the thermodynamic clusters by a single size C_{Th}.

As a Viedma ripening process runs under nearly equilibrium conditions, or rather a near equilibrium steady state, we, as in the earlier model, assume that the primary nucleation rate of crystals in the system is zero. That is, the thermodynamic clusters that are formed spontaneously will never reach the size of the critical nucleus, which is relatively large for near equilibrium conditions. The extended model thus contains three crystal sizes and is schematized in Figure 5. It is described by the set of rate (eqs 1a−1e), together with the analogous equations for the amounts of molecules with opposite sign.

$$\frac{dB^+}{dt} = aB^+(M^+ - M_{eq}^B) - bB^+ + cC^+B^+ + c_{Th}C_{Th}^+B^+ \quad (1a)$$

$$\frac{dC^+}{dt} = aC^+(M^+ - M_{eq}^C) + bB^+ - cC^+B^+ \quad (1b)$$

$$\frac{dC_{Th}^+}{dt} = a_{Th}(M^+ - M_{Th,eq}^C)(C_{Th,eq} - C_{Th}^+) - c_{Th}C_{Th}^+B^+ \quad (1c)$$

DOI: 10.1021/acs.cgd.6b00804
Cryst. Growth Des. 2016, 16, 4752−4758

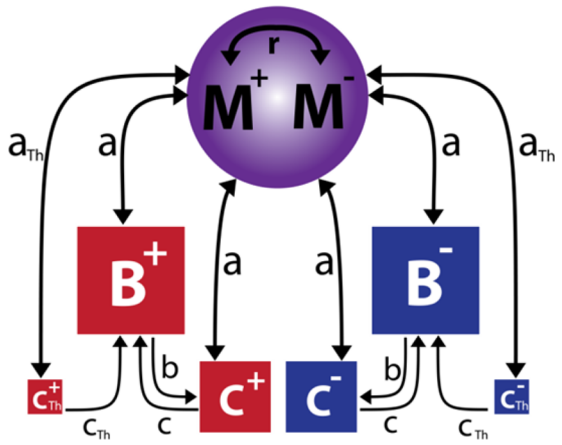

Figure 5. Schematic view of the processes involved during Viedma ripening according to the model including thermodynamic chiral clusters C_{Th}.

$$\frac{dM^+}{dt} = -aB^+(M^+ - M^B_{eq}) - aC^+(M^+ - M^C_{eq}) - a_{Th}(M^+ - M^C_{Th,eq})(C_{Th,eq} - C^+_{Th}) - r(M^+ - M^-) \quad (1d)$$

$$N = B^+ + C^+ + C^+_{Th} + M^+ + B^- + C^- + C^-_{Th} + M^- \text{ is constant} \quad (1e)$$

The thermodynamic clusters are produced spontaneously with a rate constant a_{Th}. To avoid too many parameters in the model, the production of thermodynamic clusters as a result of attrition is neglected. For the same reason, the thermodynamic clusters are assumed to be enantioselectively incorporated into the big crystals only, with rate constant c_{Th}. These additional processes will occur in reality but are not needed to derive the main effects of the thermodynamic clusters.

The number of monomers in solution when in equilibrium with the clusters, M^C_{eq}, will be larger than the equivalent M^B_{eq} for the big crystals due to the Gibbs−Thomson effect.[30] For the big crystals, the Gibbs−Thomson effect is small, and we may thus assume that M^B_{eq} corresponds to the concentration in a saturated solution. In such a saturated solution, the monomer concentration corresponds to the equilibrium number of monomers for the thermodynamic clusters as well. Therefore, $M^C_{Th,eq} = M^B_{eq}$.

The production of the thermodynamic clusters depends on the deviation of the actual number of monomers from the equilibrium number of monomers in solution, $(M^{+/-} - M^C_{Th,eq})$, a measure for the supersaturation, and on the analogous deviation in the thermodynamic clusters $(C_{Th,eq} - C^{+/-}_{Th})$. In these expressions, $C_{Th,eq}$ is the equilibrium number of molecules in the chiral thermodynamic clusters altogether. As, apart from the racemization reaction with rate r, we assume no interaction between the two enantiomers, $C^+_{Th,eq} = C^-_{Th,eq} = C_{Th,eq}$, and the value follows the Boltzmann distribution, as detailed below.

Results of the Extended Model. The deracemization process will be described by the enantiomeric excess in the solids as well as in the solution in time. For the solids, the *ee* is defined for the big crystals as

$$ee^B = \frac{B^+ - B^-}{B^+ + B^-} \quad (2)$$

and analogously for the clusters, ee^C. In principle, the thermodynamic clusters are part of the total amount of solids, but they are so small that, during sampling of the solids, they will pass the sampling filter. Therefore, the total *experimental* solids enantiomeric excess, ee_s, will in good approximation be equal to

$$ee_s = \frac{(B^+ + C^+) - (B^- + C^-)}{B^+ + C^+ + B^- + C^-} \quad (3)$$

In the solution, the *ee* of the monomers is defined as

$$ee^M = \frac{M^+ - M^-}{M^+ + M^-} \quad (4)$$

However, due to the small size of the thermodynamic clusters, the total *experimental* solution (liquid) enantiomeric excess, ee_l, will be

$$ee_l = \frac{(M^+ + C^+_{Th}) - (M^- + C^-_{Th})}{(M^+ + C^+_{Th}) + (M^- + C^-_{Th})} \quad (5)$$

For a numerical integration of the set of rate eqs (1), the rate parameters and numbers of molecules of the paper by Noorduin et al., which resulted in Figure 3, were used, i.e., a = 3.0, b = 0.5, c = 0.2, r = 2, M^B_{eq} = 1.0, and M^C_{eq} = 1.1.[27] For the additional parameters in the extended model, in the first instance, the following values were chosen: c_{Th} = 0.2, a_{Th} = 3.0, $M^C_{Th,eq} = M^B_{eq}$, and $C_{Th,eq}$ = 0.2. This choice leads to the results in Figure 6.

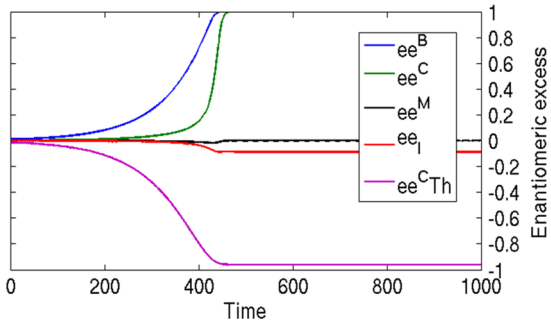

Figure 6. Evolution of the deracemization process during Viedma ripening according to the thermodynamic cluster model. a = 3.0, b = 0.5, c = 0.2, r = 2.0, M^C_{eq} = 1.1, c_{Th} = 0.2, a_{Th} = 3.0, $M^C_{Th,eq} = M^B_{eq}$ = 1.0, $C_{Th,eq}$ = 0.2, and N = 15. The enantiomeric excesses of the individual contributions are presented and the total experimental reverse solution enantiomeric excess ee_l according to eq 5.

The figure shows that a significant reverse enantiomeric excess of $ee_l \approx 0.1$ for the calculated solution sample will occur under the chosen conditions as a result of the thermodynamic clusters. The extended model can thus explain the observed persistent reverse *ee*. The enantiomeric excess of the *monomers* in the solution ee^M returns to zero in the final steady state situation as in the earlier model.

In order to understand this result, the final steady state situation of the process is depicted in Figure 7. M^+ and M^- are equal, but C^+_{Th} and C^-_{Th} are not. The '−' thermodynamic clusters only interact with M^-, but the '+' thermodynamic clusters experience the extra process of incorporation into the big crystals, leading to a lower value of C^+_{Th}. The larger value of C^-_{Th} thus leads to the persistent reverse *ee* of the solution under grinding conditions.

DOI: 10.1021/acs.cgd.6b00804
Cryst. Growth Des. 2016, 16, 4752−4758

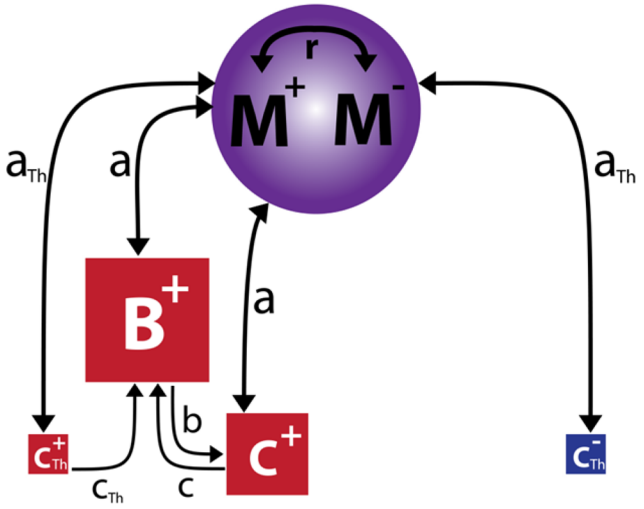

Figure 7. Final situation of a Viedma ripening experiment with one enantiomer left in the solid phase according to the thermodynamic cluster model.

Once the grinding is stopped, corresponding to $b = 0$ in eqs (1), the clusters C^+ in Figure 7 will all be dissolved or incorporated into the crystals B^+. Moreover, Ostwald ripening then results in less crystals of increasingly larger size, reducing the chance of incorporation of the thermodynamic clusters of the same enantiomer and thus leading to a decrease in the measured ee_l. When the grinding is completely stopped, the slurry becomes quickly inhomogeneous and with that the sampling unreliable. We tried to observe the change in ee_l by reducing the rotation rate of the stirring bar from 360 rpm down to 50 rpm. This resulted in a reduction of the ee_l value by approximately 35%.

Figure 2 shows that the reverse enantiomeric excess for the solution samples is, within the experimental uncertainty, independent of the filter size (1, 4, or 10 μm) used for sampling. This is an indication for a bimodal size distribution for the thermodynamic clusters on the one hand and the big crystals and the clusters due to the attrition on the other hand.

Estimation of Thermodynamic Cluster Concentration. To get an indication of the equilibrium number of molecules in the clusters $C_{Th,eq}$, we can make an estimation based on classical nucleation theory.[31] For the equilibrium concentration $C(n)$ of clusters consisting of $n > 1$ molecules in an equilibrium situation, the Boltzmann distribution at temperature T results in

$$C(n) = C_1 \exp\left[-\frac{W(n)}{kT}\right] \tag{6}$$

where k is the Boltzmann constant and C_1 is the concentration of solute monomers in the solution. The work $W(n)$ needed for the creation of a cluster of size n molecules is determined by only the surface energy of the cluster when we assume that the structure of the cluster is identical to that of a bulk crystal, as, in that case, the chemical potential of the molecules in the interior of the cluster μ_s is equal to that of the monomers in a saturated solution μ_l.

Assuming only spherical clusters with radius $R(n)$, with isotropic specific surface energy σ and a molecular volume v_0, we can determine the work as

$$W(n) = 4\pi R(n)^2\sigma = (36\pi)^{1/3} v_0^{2/3} \sigma n^{2/3} \tag{7}$$

This is a crude assumption for small clusters. Nevertheless, in terms of the variables used in the extended model, eq 6 implies that, in thermodynamic equilibrium

$$\frac{C_{Th}^+}{M^+} = \frac{C_{Th}^-}{M^-} = \frac{\sum_{n=2}^{\infty} nC(n)}{C_1} = \frac{\sum_{n=2}^{\infty} n \exp\left[-\frac{(36\pi)^{1/3} v_0^{2/3} \sigma n^{2/3}}{kT}\right]}{C_1} \tag{8}$$

The unit cell volume for the case of alanine 4-chlorobenzenesulfonic acid, containing $Z = 4$ molecules, is $V = 1.226$ nm^3, resulting in a molecular volume $v_0 = 0.31$ nm^3.[32] In Figure 8,

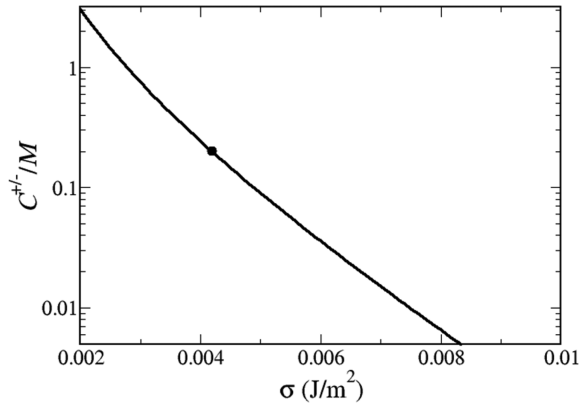

Figure 8. Expected value for $C_{Th}^{+/-}/M$ is plotted, using eq 8, as a function of the isotropic specific surface energy σ for $v_0 = 0.31$ nm^3 and $T = 340$ K. The experimental value $ee_l = 0.20$ corresponding to $\sigma = 4.2$ mJ/m^2 is indicated.

the expected value for $C_{Th}^{+/-}/M$ is plotted, using eq 8, as a function of the isotropic specific surface energy σ for this molecular volume at the experimental temperature of 340 K.

For the parameter values used in Figure 6, in the steady state regime, where $M^+ = M^- = M$ and the enantiomeric excess of the thermodynamic clusters $ee_{Th}^C \approx -1.0$, implying that $C_{Th}^+ \ll C_{Th}^-$, eq 5 becomes

$$ee_l^{st.st.} = \frac{C_{Th}^+ - C_{Th}^-}{2M + C_{Th}^+ + C_{Th}^-} \approx -\frac{C_{Th}^-}{2M + C_{Th}^-} \tag{9}$$

In Figure 2, the steady state experimental solution reverse enantiomeric excess $ee_l^{st.st.} \approx -0.09$. Solving eq 9 for this value and assuming $C_{Th}^- \ll M$ results in $C_{Th}^-/M^- \approx 0.20$. Setting eq 8 equal to this value and solving it at the temperature of the experiment ($T = 340$ K), we find a value for the specific surface energy of $\sigma = 4.2$ mJ/m^2.

Alternatively, the specific surface energy σ can be estimated using the relation between the surface energy and the solubility proposed by Mersmann, based on thermodynamics and tested for aqueous solutions of various salts[33]

$$\sigma = \frac{2}{(36\pi)^{1/3}} (c_S N_A)^{2/3} kT \ln\left[\frac{c_S}{c_L}\right] \tag{10}$$

where c_S and c_L are the equilibrium concentration in the solid and the solution, respectively, and N_A is Avogadro's number. Equation 10 is equally well applicable in the case of pure acetic acid as a solvent. The solubility of the amino acid salt in pure acetic acid is 230−260 mg/mL at the experimental temper-

DOI: 10.1021/acs.cgd.6b00804
Cryst. Growth Des. 2016, 16, 4752−4758

ature. Using eq 10, the specific surface energy is estimated to be $\sigma = 7.7$ mJ/m^2 for $C_l = 250$ mg/mL. This result is of the same order as the value of $\sigma = 4.2$ mJ/m^2 and shows that our model gives reasonable results.

Equation 8 also provides the average number of molecules in the thermodynamic clusters. This number is estimated to be roughly equal to 5. We can compare this number with an estimation of cluster sizes in supersaturated solutions by Ginde and Myerson.[34] In their paper, the authors interpreted experimental concentration gradient data of various published studies as well as data of their own and found values between 2 and 100 molecules for supersaturations $S = 1$ and higher. The presently found average of 5 molecules is in line with this result, especially as in our case, we have a (nearly) equilibrium situation.

The sizes of the thermodynamic clusters are so small that they will all be collected in a filtered sample of the solution. On the other hand, these clusters together contain enough molecules as compared to the equilibrium solubility to give rise to the observed reverse enantiomeric excess. The relatively low surface energy E_σ needed for the buildup of a nonzero steady state solution reverse enantiomeric excess is achieved in the amino acid salt by a relatively low value of the specific surface energy, despite the large molecular volume.

CONCLUSION

During Viedma ripening experiments on alanine 4-chlorobenzenesulfonic acid, the solution shows a small enantiomeric excess ee_l with the reverse sign as compared to the solid state enantiomeric excess. Even after complete deracemization, this reverse solution *ee* is persistent as long as the grinding is maintained. Models published up to now cannot explain this behavior. The present model that includes thermodynamic chiral clusters and their incorporation into larger crystals of the same chirality shows a reverse solution enantiomeric excess. The size of the reverse ee_l is in good agreement with the estimated subcritical cluster distribution calculated on the basis of a Boltzmann distribution and classical nucleation theory. Therefore, this result reinforces the essence of the cluster incorporation mechanism in Viedma ripening once more.

Besides Viedma ripening, thermal cycling has been found as an alternative for deracemizing racemic conglomerates without grinding.[35] Growth rate dispersion has been proposed to explain the deracemization in thermal cycling.[36] In a recent paper, Uwaha adapted his cluster model for Viedma ripening to explain the deracemization observed in thermal cycling experiments.[37] It will be interesting, therefore, to adapt the model of the present paper to the case of thermal cycling and to test its validity in such an experiment.

EXPERIMENTAL DETAILS

Deracemization Experiment. An alanine 4-chlorobenzenesulfonic acid (**Ala-CBS**) deracemization experiment was typically conducted with (*RS*)-**Ala** (1.4 g), (*R*)- or (*S*)-**Ala** (0.12 g), and ca. 3 g of 4-chlorobenzenesulfonic acid, corresponding to 90% of the molar amounts of alanine. These amounts should result in a 10% excess of free alanine to ensure the racemization reaction in solution. Because of the lesser purity of 4-chlorobenzenesulfonic acid and its hygroscopicity, the excess will be somewhat higher (about 17%). To produce the conglomerate, these compounds were stirred in 10 mL of acetic acid in a 25 mL round-bottom flask with an oval PTFE-coated magnetic stir bar (L 20 mm, Ø 10 mm) in the presence of ca. 7.5 g of glass beads (Ø ca. 2 mm, VWR international) at 70 °C. The racemization reaction was started by adding 200 mg of salicylaldehyde. Samples were taken over time. The chemicals were purchased from Sigma-Aldrich ((*RS*)-**Ala** (99%), (*S*)-**Ala** (98%), (*R*)-**Ala** (98%), 4-chlorobenzenesulfonic acid (90%), and salicylaldehyde (98%)), except for glacial acetic acid, which was purchased from J.T. Baker (99–100%).

Sampling. For the first sampling method used, for each sample including the initial one, 0.5 mL of the slurry was removed with a pipet and vacuum filtered as fast as possible at room temperature on a P4 glass filter (Ø 10 mm). The residue was washed with 2 mL of acetone to remove the adhering racemic solution and dried. The sample for the determination of the solution *ee* was received during the filtration process by collecting the filtrate and the acetone. The liquids were evaporated and the resulting crystals dried.

For the second method, the samples were extracted directly from the round-bottom flask with a 1 mL syringe equipped with a poroplast cannula filter (10, 4, or 1 μm) (Quality Lab Accessories). The solution was immediately transferred into a small vial. Acetone was added to the solution to reduce the temperature rapidly and to thereby terminate the racemization reaction. Crystallization occurred instantaneously after adding the antisolvent acetone.

Determination of the *ee* of the Solid Samples by Chiral HPLC Analysis. ***Ala-CBS*** *Sample Preparation.* 3 mg of solid in 1 mL of Milli Q water, injection volume 10 μL, HPLC column Chirobiotic T (250 × 4.6 mm ID), 5 μm, Astec; eluent acetonitrile/water 70/30 v/v, flow 1 mL/min, detection $\lambda = 205$ nm. Retention times (*S*)-**Ala-CBS** 11.1 min, (*R*)-**Ala-CBS** 12.3 min.

AUTHOR INFORMATION

Corresponding Author

*E-mail: H.Meekes@science.ru.nl.

Notes

The authors declare no competing financial interest.

ACKNOWLEDGMENTS

Financial support for this work was provided by The Netherlands Organization for Scientific Research (NWO).

REFERENCES

(1) Viedma, C. *Phys. Rev. Lett.* **2005**, *94*, 065504.
(2) Sögötoglu, L. C.; Steendam, R. E.; Meekes, H.; Vlieg, E.; Rutjes, F. P. J. T. *Chem. Soc. Rev.* **2015**, *44*, 6723–6732.
(3) Viedma, C. *Cryst. Growth Des.* **2007**, *7*, 553–556.
(4) Cheung, P. S. M.; Gagnon, J.; Surprenant, J.; Tao, Y.; Xu, H. W.; Cuccia, L. A. *Chem. Commun.* **2008**, 987–989.
(5) McLaughlin, D. T.; Nguyen, T. P. T.; Mengnjo, L.; Bian, C.; Leung, Y. H.; Goodfellow, E.; Ramrup, P.; Woo, S.; Cuccia, L. A. *Cryst. Growth Des.* **2014**, *14*, 1067–1076.
(6) Xiouras, C.; Van Aeken, J.; Panis, J.; Ter Horst, J. H.; Van Gerven, T.; Stefanidis, G. D. *Cryst. Growth Des.* **2015**, *15*, 5476–5484.
(7) Noorduin, W. L.; Izumi, T.; Millemaggi, A.; Leeman, M.; Meekes, H.; Van Enckevort, W. J. P.; Kellogg, R. M.; Kaptein, B.; Vlieg, E.; Blackmond, D. G. *J. Am. Chem. Soc.* **2008**, *130*, 1158–1159.
(8) Noorduin, W. L.; Bode, A. A. C.; van der Meijden, M.; Meekes, H.; van Etteger, A. F.; van Enckevort, W. J. P.; Christianen, P. C. M.; Kaptein, B.; Kellogg, R. M.; Rasing, T.; Vlieg, E. *Nat. Chem.* **2009**, *1*, 729–732.
(9) Viedma, C.; Ortiz, J. E.; de Torres, T.; Izumi, T.; Blackmond, D. G. *J. Am. Chem. Soc.* **2008**, *130*, 15274–15275.
(10) Kaptein, B.; Noorduin, W. L.; Meekes, H.; van Enckevort, W. J. P.; Kellogg, R. M.; Vlieg, E. *Angew. Chem., Int. Ed.* **2008**, *47*, 7226–7229.
(11) Noorduin, W. L.; Kaptein, B.; Meekes, H.; van Enckevort, W. J. P.; Kellogg, R. M.; Vlieg, E. *Angew. Chem., Int. Ed.* **2009**, *48*, 4581–4583.
(12) van der Meijden, M. W.; Leeman, M.; Gelens, E.; Noorduin, W. L.; Meekes, H.; van Enckevort, W. J. P.; Kaptein, B.; Vlieg, E.; Kellogg, R. M. *Org. Process Res. Dev.* **2009**, *13*, 1195–1198.

DOI: 10.1021/acs.cgd.6b00804
Cryst. Growth Des. 2016, 16, 4752–4758

(13) Leeman, M.; Noorduin, W. L.; Millemaggi, A.; Vlieg, E.; Meekes, H.; van Enckevort, W. J. P.; Kaptein, B.; Kellogg, R. M. *CrystEngComm* **2010**, *12*, 2051−2053.
(14) Spix, L.; Meekes, H.; Blaauw, R. H.; van Enckevort, W. J. P.; Vlieg, E. *Cryst. Growth Des.* **2012**, *12*, 5796−5799.
(15) Hein, J. E.; Cao, B. H.; Viedma, C.; Kellogg, R. M.; Blackmond, D. G. *J. Am. Chem. Soc.* **2012**, *134*, 12629−12636.
(16) Rybak, W. K. *Tetrahedron: Asymmetry* **2008**, *19*, 2234−2239.
(17) Tsogoeva, S. B.; Wei, S.; Freund, M.; Mauksch, M. *Angew. Chem., Int. Ed.* **2009**, *48*, 590−594.
(18) Flock, A. M.; Reucher, C. M. M.; Bolm, C. *Chem.—Eur. J.* **2010**, *16*, 3918−3921.
(19) Spix, L.; Alfring, A.; Meekes, H.; van Enckevort, W. J. P.; Vlieg, E. *Cryst. Growth Des.* **2014**, *14*, 1744−1748.
(20) Steendam, R. R. E.; Brouwer, M. C. T.; Huijs, E. M. E.; Kulka, M. W.; Meekes, H.; van Enckevort, W. J. P.; Raap, J.; Rutjes, F. P. J. T.; Vlieg, E. *Chem.—Eur. J.* **2014**, *20*, 13527−13530.
(21) Steendam, R. R. E.; Dickhout, J.; van Enckevort, W. J. P.; Meekes, H.; Raap, J.; Rutjes, F. P. J. T.; Vlieg, E. *Cryst. Growth Des.* **2015**, *15*, 1975−1982.
(22) Noorduin, W. L.; Meekes, H.; van Enckevort, W. J. P.; Millemaggi, A.; Leeman, M.; Kaptein, B.; Kellogg, R. M.; Vlieg, E. *Angew. Chem., Int. Ed.* **2008**, *47*, 6445−6447.
(23) Uwaha, M. *J. Phys. Soc. Jpn.* **2008**, *77*, 083802.
(24) Uwaha, M. *J. Cryst. Growth* **2011**, *318*, 89−92.
(25) Saito, Y.; Hyuga, H. *Rev. Mod. Phys.* **2013**, *85*, 603−621.
(26) Noorduin, W. L.; Meekes, H.; Bode, A. A. C.; van Enckevort, W. J. P.; Kaptein, B.; Kellogg, R. M.; Vlieg, E. *Cryst. Growth Des.* **2008**, *8*, 1675−1681.
(27) Noorduin, W. L.; van Enckevort, W. J. P.; Meekes, H.; Kaptein, B.; Kellogg, R. M.; Tully, J. C.; McBride, J. M.; Vlieg, E. *Angew. Chem., Int. Ed.* **2010**, *49*, 8435−8438.
(28) Iggland, M.; Mazzotti, M. *Cryst. Growth Des.* **2011**, *11*, 4611−4622.
(29) Gherase, D.; Conroy, D.; Matar, O. K.; Blackmond, D. G. *Cryst. Growth Des.* **2014**, *14*, 928−937.
(30) Thomson, S. W. *London, Edinburgh Dublin Philos. Mag. J. Sci.* **1871**, *42*, 448−452.
(31) Kashchiev, D. *Nucleation*; Butterworth-Heinemann: Oxford, U.K., 2000.
(32) Kimoto, H.; Saigo, K.; Ohashi, Y.; Hasegawa, M. *Bull. Chem. Soc. Jpn.* **1989**, *62*, 2189−2195.
(33) Mersmann, A. *J. Cryst. Growth* **1990**, *102*, 841−847.
(34) Ginde, R. M.; Myerson, A. S. *J. Cryst. Growth* **1992**, *116*, 41−47.
(35) Suwannasang, K.; Flood, A. E.; Rougeot, C.; Coquerel, G. *Cryst. Growth Des.* **2013**, *13*, 3498−3504.
(36) Suwannasang, K.; Coquerel, G.; Rougeot, C.; Flood, A. E. *Chem. Eng. Technol.* **2014**, *37*, 1329−1339.
(37) Katsuno, H.; Uwaha, M. *Phys. Rev. E: Stat. Phys., Plasmas, Fluids, Relat. Interdiscip. Top.* **2016**, *93*, 013002.

DOI: 10.1021/acs.cgd.6b00804
Cryst. Growth Des. 2016, 16, 4752−4758